Chinese Journal of Physics 100 (2026) 95–102

Contents lists available at ScienceDirect

Chinese Journal of Physics

journal homepage: www.sciencedirect.com/journal/chinese-journal-of-physics

Tunable spin-wave resonance and chirality control in concentric nanotori for advanced spintronic applications

Eduardo Saavedra [a,*], Ulises J. Guevara [b], Carlos Saji [a], Tamara González-Vega [c], Pablo Díaz [d], Laura M. Pérez [e]

[a] Departamento de Física, Universidad de Santiago de Chile, 9170124, Santiago, Chile
[b] Vicerrectoría de Investigación y Postgrado, Universidad de La Serena, La Serena, 1700000, Chile
[c] Facultad de Ciencias de la Vida, Universidad Viña del Mar, Agua Santa 7055, Rodelillo, Viña del Mar, 2572007, Chile
[d] Departamento de Ciencias Físicas, Universidad de La Frontera, Temuco, Chile
[e] Departamento de Ingeniería Industrial y de Sistemas, CEDENNA, Universidad de Tarapacá, Casilla 7D, Arica, 1000000, Chile

ARTICLE INFO

Keywords:
Tunable spin-wave resonance
Concentric nanotori
Chirality control

ABSTRACT

We investigate the spin-wave dynamics in concentric magnetic nanotori through micromagnetic simulations under perpendicular pulsed magnetic fields, using the free software MuMax3. These 3D nanostructures can host homochiral and heterochiral vortex configurations, whose spin-wave spectra strongly depend on the magnetostatic coupling parameter δ. In homochiral systems, resonance modes converge as δ increases, while in heterochiral systems, they diverge. Two distinct modes are identified: one associated with the outer surfaces of the tori and another with the inner torus. A central result is the demonstration of reversible transitions between homochiral and heterochiral vortex states using oscillating magnetic fields. The switching behavior and resonance properties vary with the coupling parameter δ, revealing the system's dynamic versatility. This tunable chirality control positions concentric nanotori as promising candidates for future spintronic devices, enabling new opportunities for magnonic logic, non-volatile memory, and neuromorphic architectures. This work enhances the integration of 3D magnetic geometries with dynamic control, paving the way for applications in topological information processing and reconfigurable magnetic computing.

1. Introduction

In recent decades, significant progress has been made in understanding the static and dynamic magnetic properties of nanoscale systems with complex geometries. A broad variety of two- and three-dimensional nanostructures-such as disks [1–3], rings [4,5], thin films and multilayer structures [6–11], and spheres [12,13]-have been extensively investigated as versatile platforms for hosting diverse magnetic states. In contrast, toroidal geometries [14–17] have only recently begun to attract attention, owing to their distinctive curvature-induced effects that give rise to nontrivial magnetization textures. By precisely tailoring parameters such as diameter, thickness, and curvature, these nanostructures are capable of stabilizing a variety of complex magnetization textures.

Among the most notable configurations found in such systems are skyrmions [4], bimerons [1,2], onion states [17], hopfions [15], and magnetic vortices [5,12,14,16–18], as well as other non-trivial magnetic textures [3]. In particular, magnetic vortices stand out due to their topological character and are defined by two independent degrees of freedom: chirality and polarity. Chirality describes

* Corresponding author.
E-mail address: eduardo.saavedra.d@usach.cl (E. Saavedra).

https://doi.org/10.1016/j.cjph.2025.12.035
Received 7 August 2025; Received in revised form 23 December 2025; Accepted 28 December 2025
Available online 1 January 2026
0577-9073/

the rotational sense of the in-plane magnetization-either clockwise or counterclockwise-while polarity refers to the orientation of the magnetization at the vortex core along the out-of-plane (z) direction, taking values of $+1$ or -1.

The controlled formation and manipulation of these topologically distinct states have unlocked new possibilities for technological applications. Magnetic vortex configurations, in particular, are being explored as functional units in a wide array of devices, including magnetic random access memory (MRAM) [19], highly sensitive magnetic sensors [20], high-density data storage platforms [21–23], reconfigurable logic gates [24,25], magnetic valves [18,26], and nanoscale magnetic oscillators [27]. These advances not only demonstrate the versatility of magnetic nanostructures but also highlight the role of geometry and topology in the development of future spintronic technologies.

Previous studies have highlighted the critical role of magnetostatic interactions and geometrical parameters in determining the spin-wave dynamics of concentric magnetic nanostructures. McKeever et al. [28] investigated the high-frequency behavior of concentric permalloy nanorings in vortex states using micromagnetic simulations. Their results revealed that the resonance frequencies are highly sensitive to the inter-ring magnetostatic coupling, which can be modulated by adjusting the width and spacing of the rings. Additionally, they reported that the spatial localization of the uniform resonance mode changes systematically with the separation between rings, underscoring the spatial tunability of the magnetic response.

In a related study, Sahu et al. [29] analyzed both static and dynamic magnetic properties of similar concentric nanoring systems. They observed that, for most geometries, the magnetic hysteresis loops exhibit negligible remanence and coercivity, suggesting soft magnetic behavior. Dynamically, they found that in-plane magnetic field pulses primarily excite azimuthal spin-wave modes, with the number of resonance peaks increasing proportionally with the number of rings. Furthermore, the resonant frequencies were shown to depend on the magnetic ground state of the system, indicating a strong interplay between static configuration and dynamic excitation.

We know that the mass production of toroidal nanoparticles faces a delicate balance between structural precision and industrial feasibility. While nanoimprint lithography (NIL) allows for the replication of nanostructures with high fidelity and low cost, limitations such as junction defects and optical leakage reduce uniformity over large areas [30]. Therefore, three-dimensional fabrication techniques, such as two-photon lithography (TPL) and focused electron beam-induced deposition (FEBID), allow for the creation of complex structures and topological control, but their high cost and low throughput restrict their use to laboratory-scale prototypes [31]. In the biomedical field, toroidal magnetite nanoparticles stand out for their "on/off" magnetization behavior; however, hydrothermal synthesis methods still exhibit low reproducibility and limited scalability [17]. In short, there is a clear need for 3D manufacturing with the efficiency of replicative methods, for standardized large-scale manufacturing of functional toroidal nanostructures.

Building upon this line of research, Saavedra et al. [16] extended the analysis to concentric nanotori, exploring the role of vortex chirality in shaping the spin-wave resonance spectra. Using micromagnetic simulations under in-plane pulsed excitation, they demonstrated that poloidal resonance modes are strongly influenced by the relative chirality of the vortices hosted in each torus. Specifically, they showed that the frequency spectra differ markedly between homochiral and heterochiral configurations, and that this spectral structure can be tuned by varying the inter-torus distance. These findings underscore the importance of topological features such as chirality in modulating magnetization dynamics, further reinforcing the potential of such architectures in the design of advanced spintronic and magnonic devices.

This study investigates the dynamic magnetic properties of two concentric nanotori nanostructures, enabling homochiral and heterochiral vortex configurations, with a focus on their frequency spectra and spatial resonance modes under perpendicular microwave excitation. By applying oscillating magnetic field pulses along the z-axis at the frequency of the spin wave mode and adjusting the intensity of the magnetic field in the sub-nanosecond range, it is possible to switch between heterochiral and homochiral vortex states. This control over chirality has significant implications for the development of advanced magnetic materials and devices, potentially improving their performance in applications such as data storage, spintronics, and magnetic sensing technologies.

2. Model and methodology

The system under study consists of two concentric magnetic nanotori, geometrically characterized by a fixed toroidal radius $R_{T1} = 226$ nm for the outer torus, and a variable toroidal radius R_{T2} for the inner one. The relationship between these radii is governed by the following expression:

$$R_{T2} = \delta\left(R_{T1} - 3r_p\right) + r_p$$

where $r_p = 24\,\text{nm}$ denotes the poloidal radius, which remains identical for both nanotori. The parameter $\delta \in [0, 1]$ is a dimensionless proportionality factor that controls the separation and coupling strength between the inner and outer tori. When $\delta = 0$, the inner torus collapses to its minimum size $R_{T2} = r_p$, while $\delta = 1$ corresponds to the condition where the inner torus just touches the interior surface of the outer torus, i.e., $R_{T2} = R_{T1} - 2r_p$, as illustrated in Fig. 1.

This parametrization provides a continuous and controllable framework to tune the spatial configuration and magnetostatic interaction between the tori. Such a setup enables a systematic exploration of the effects of geometric coupling on the spin-wave dynamics and vortex chirality within three-dimensional nanomagnetic systems.

All micromagnetic simulations in this work were performed using the open-source software package MuMax3 [32], which numerically solves the Landau-Lifshitz-Gilbert (LLG) equation by means of the finite difference method. This approach allows for the precise modeling of magnetization dynamics in complex geometries, such as the concentric nanotori studied here.

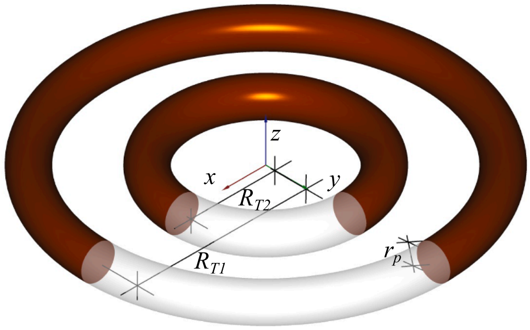

Fig. 1. Schematic representations of two concentric nanotori used in the micromagnetic simulations, where R_{T2} represents the toroidal radius of the inner toroid, and R_{T1} represents the toroidal radius of the outer toroid andthe parameter r_p are the same for both nanotori.

The LLG equation governs the time evolution of the normalized magnetization vector $\mathbf{m} = \vec{M}/M_s$, where $\vec{M}$ is the local magnetization and M_s denotes the saturation magnetization. The equation is expressed as follows:

$$\frac{d\mathbf{m}}{dt} = -\gamma(\mathbf{m} \times \mathbf{H}_{\rm eff}) + \alpha\left(\mathbf{m} \times \frac{d\mathbf{m}}{dt}\right) \tag{1}$$

where γ is the gyromagnetic ratio and α is the Gilbert damping constant, which characterizes the rate at which the system dissipates energy and relaxes toward equilibrium. The effective magnetic field $\mathbf{H}_{\rm eff}$ encapsulates all local and nonlocal interactions and is obtained from the variational derivative of the total magnetic energy density ε with respect to $\mathbf{m}$, expressed as:

$$\mathbf{H}_{\rm eff} = -\frac{1}{\mu_0 M_s}\frac{\delta\varepsilon}{\delta\mathbf{m}}, \tag{2}$$

where μ_0 is the vacuum permeability. The total energy density ε includes contributions from the exchange interaction $\varepsilon_{\rm ex}$, magnetostatic (dipolar) interaction $\varepsilon_{\rm d}$, and the Zeeman interaction $\varepsilon_{\rm Z}$, such that:

$$\varepsilon = \varepsilon_{\rm ex} + \varepsilon_{\rm d} + \varepsilon_{\rm Z}.$$

To ensure an accurate representation of the curved geometry of the concentric nanotori and to minimize artificial boundary effects, the computational domain was discretized using a uniform mesh size of $2 \times 2 \times 2$ nm^3, which provides an acceptable spatial resolution well-suited for capturing the magnetization dynamics in three-dimensional nanostructures [33,34]. This mesh size is sufficiently small to resolve the intricate features of the vortex configurations while maintaining computational efficiency. To mitigate staircase effects arising from cubic cells, the edges were smoothed. The smoothed edge volume is determined by averaging p^3 samples per cell, where p is the input parameter for the function. Given that the geometry is a curved shape, the "SmoothEdges" function was set to its maximum value of 8.

To validate the robustness of the results, additional simulations were conducted using an even finer discretization of $1 \times 1 \times 1$ nm^3. These higher-resolution calculations showed negligible differences, with deviations in the results remaining below 1% (see Fig. S2 in the supplementary material), confirming the convergence and reliability of the chosen mesh.

The magnetic parameters used in the simulations correspond to those of Permalloy, a soft magnetic material commonly employed in nanomagnetism studies. Specifically, we used a saturation magnetization of $M_s = 800 \times 10^3$ A m^{-1}, an exchange stiffness constant of $A = 1.30 \times 10^{-11}$ J m^{-1} [29,34], and assumed a vanishing magnetocrystalline anisotropy. All simulations were conducted at zero Kelvin (i.e., no stochastic thermal field was considered in the effective field, H_{eff}). A comparative analysis of the dynamic susceptibility spectra for each magnetic configuration is presented in Figure S8, where we found that the differences were minimal, primarily attributed to the stochastic noise introduced by the temperature function in the Mumax3 software.

In the first part of our calculations, we investigated the impact of the δ interaction parameter on two distinct magnetic configurations: homochiral and heterochiral vortices within magnetic systems. Homochiral vortices are characterized by having the same chirality, whereas heterochiral vortices exhibit different chiralities (see Fig. S1 in the Supplementary Material). To achieve this, the magnetic configuration is established, and the final state is obtained by integrating the Landau-Lifshitz-Gilbert (LLG) equation until the torque reaches 10^{-4} T [35–37]. After convergence, a 100 ns time minimization step damps spin waves, stabilizing the configuration [38]. In the relaxation process, we considered a damping parameter $\alpha = 0.5$ [39].

In the second part of our calculations, we determined the resonance frequencies associated with the homochiral and heterochiral magnetic vortex configurations. To excite these modes and examine the influence of the interaction parameter δ, we applied a broadband magnetic field pulse along the z-axis of the form $\mathbf{h}(t) = h_0 \cdot \mathrm{sinc}[2\pi f_{\max}(t - t_0)]\,\hat{\mathbf{z}}$ [39,40], where $h_0 = 1$ mT, $f_{\max} = 25$ GHz, and $t_0 = 1$ ns. To accurately resolve the system's resonant response, we employed a low damping constant of $\alpha = 0.008$ during this stage [41]. The amplitude of excitation was chosen to ensure that the system remained within the linear response regime [42].

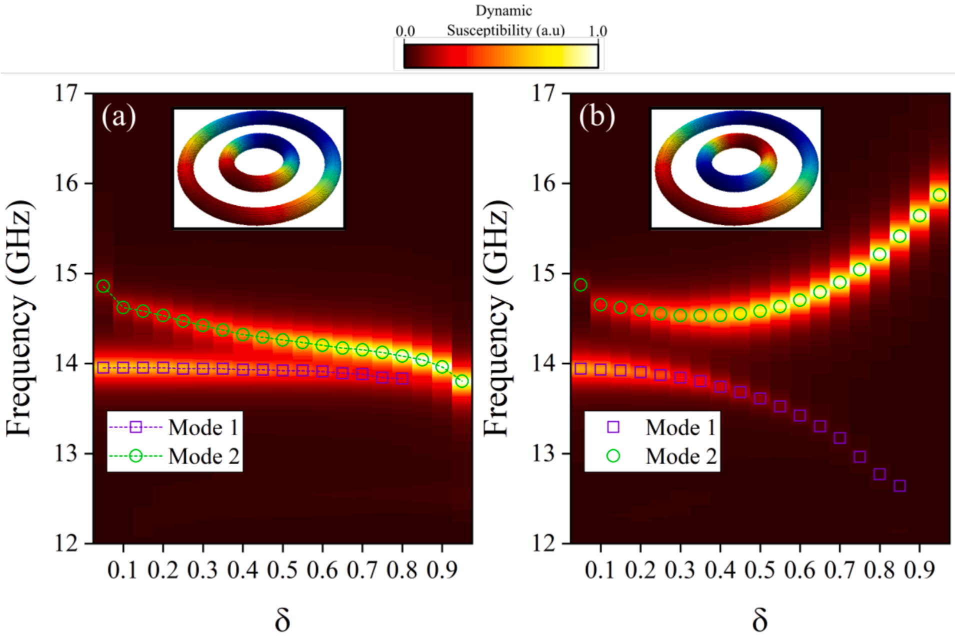

Fig. 2. Amplitude maps of the dynamic susceptibility spectra as a function of the interaction parameter δ for: (a) homochiral vortex configurations and (b) heterochiral vortex configurations.

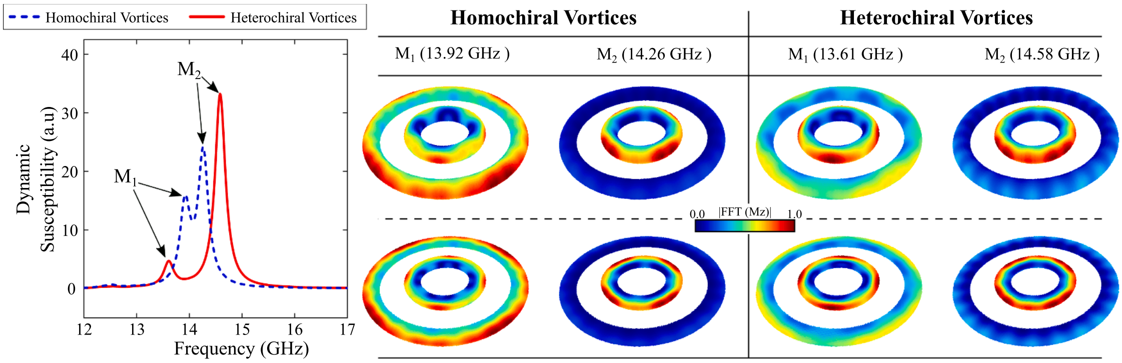

Fig. 3. Dynamic susceptibility and spatial distribution of the excited spin-waves modes in two concentric nanotori for $\delta = 0.5$. The color code in the figures at the right represents the amplitude of the FFT on the z-component of the magnetization field. The top row represents a surface of nanostructures, while the bottom row represents a slice in the xy plane.

Magnetization dynamics was simulated over a time window of 100 ns, with data recorded every 20 ps, yielding a spectral resolution of 0.01 GHz.

The dynamic susceptibility spectra χ'', corresponding to the imaginary part of the magnetic susceptibility, were obtained by dividing the fast Fourier transform (FFT) of the magnetization response $M(t)$ by the FFT of the excitation field $h(t)$ [43,44]. To spatially resolve the excited spin-wave modes, we reconstructed the temporal Fourier image of the magnetization for each computational cell. This was calculated as $\tilde{m}(r_{ijk}, f_n) = \mathrm{DFT}_t\left(m(r_{ijk}, t)\right)$, where DFT_t denotes the discrete-time Fourier transform, ijk indicates the spatial coordinates x, y, z, and n corresponds to the frequency index in the power spectrum.

3. Results and discussion

Fig. 2 presents the amplitude maps of the dynamic susceptibility spectra for each value of the interaction parameter δ from 0.05 to 0.95. For each magnetic configuration, two well-defined resonance peaks are observed. Notably, in the case of two homochiral vortices (Fig. 2(a)), the resonance modes appear between approximately 14 and 15 GHz and gradually merge into a single mode as δ increases up to 0.95. In contrast, for a heterochiral system (Fig. 2(b)), the spectra initially exhibit two distinct modes, which progressively diverge as δ approaches 0.95.

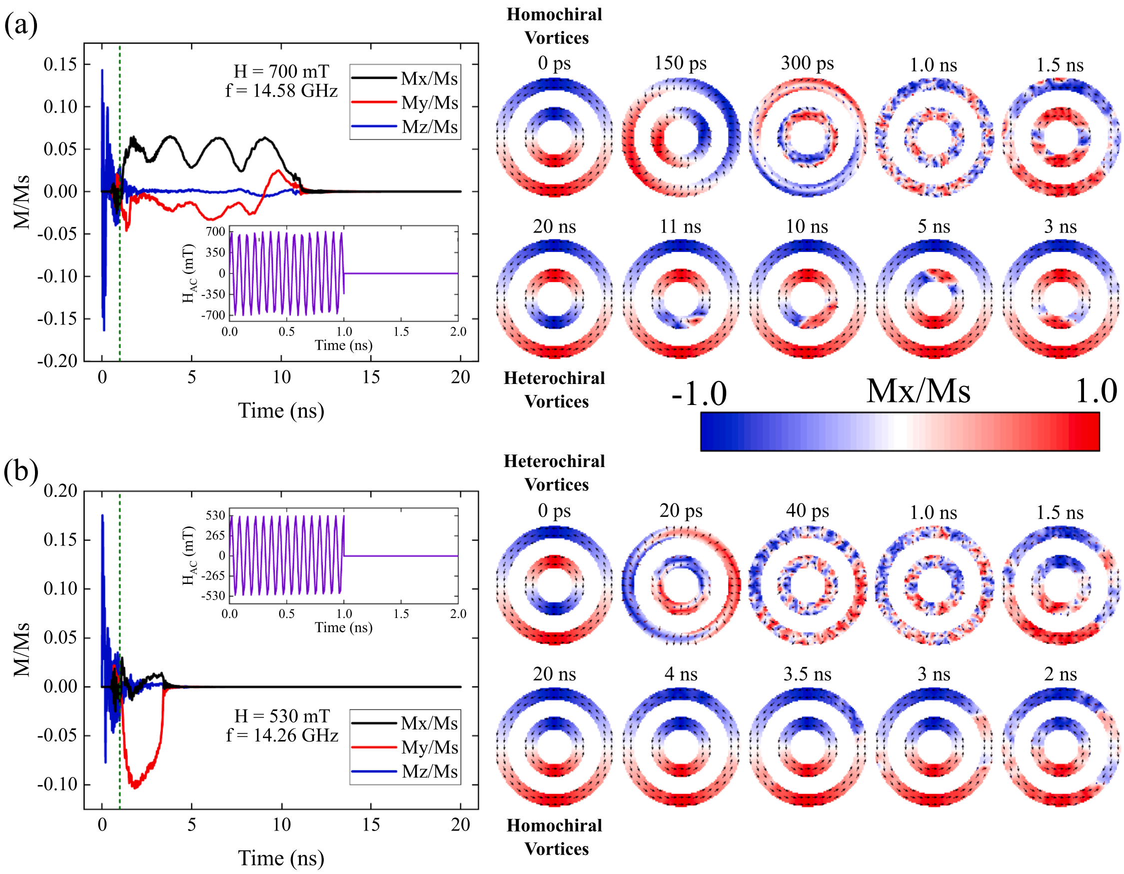

Fig. 4. (a) Transformation from homochiral to heterochiral vortices for $\delta = 0.5$. (b) Transformation from heterochiral to homochiral vortices for $\delta = 0.5$.

The left-hand graph of Fig. 3 shows the dynamic susceptibility profiles for both homochiral vortex configurations (blue dashed line) and heterochiral vortices (red line), for the case $\delta = 0.5$ (This case corresponds to an intermediate magnetic interaction regime due to a center-to-center distance of 2.5 times the poloidal diameter). where the peaks correspond to the system's resonance frequencies. In addition, the center and right panels present the spatial distribution profiles of the fast Fourier transform of the z component of the magnetization for each cell, using a color scale. The top row represents a surface of nanostructures, while the bottom row represents a slice in the xy plane. Two distinct resonance modes are observed for both homochiral (central panels) and heterochiral (right panels) vortex configurations. The first mode, labeled M_1, corresponds predominantly to the excitation of magnetic moments located on the outer surfaces of both nanotorii. In contrast, the second mode, M_2, is mainly associated with the excitation of magnetic moments localized on the inner torus.

This behavior is consistent with the dynamics observed in an isolated single torus (see Supplementary Material, Fig. S3), where two modes are also present. The first mode, M_a, appears at low intensity and within a frequency range between 13 and 14 GHz. It arises from the excitation of both the inner and outer surfaces of the torus and is barely noticeable when compared to the second, more intense mode. This latter mode, labeled M_b, is observed between 14 and 15 GHz and is primarily attributed to the excitation of magnetic moments located exclusively on the outer surface of the torus. Notably, this high-intensity mode (M_b) is the one that also manifests in the dynamics of the concentric nanotorus system.

To evaluate the scalability of the proposed system, additional micromagnetic simulations were carried out for $\delta = 0.5$ using progressively larger computational domains, ranging from $500 \times 500 \times 50$ nm^3 to $800 \times 800 \times 80$ nm^3, while maintaining a cell size of 2 nm. As illustrated in Fig. S7 in Supplementary Material, the resonance peaks exhibit only slight frequency shifts-less than 1%-as the system size increases.

This invariance confirms that the spin-wave dynamics and chirality-dependent resonance modes are robust against scaling, highlighting the potential of concentric nanotori as scalable building blocks for magnonic and spintronic architectures.

Next, it is shown that it is possible transformation from homochiral vortices to heterochiral vortices and viceversa by applying an oscillating magnetic field along the z-direction, given by $B_z = B_0 \, sin(2\pi f t)$, where B_0 is the amplitude of the magnetic field and f corresponds to the frequency of the resonance mode (M_2) of the desired final configuration. This mode is mainly localized on the inner torus, where chirality reversal occurs, and thus represents the most efficient channel for driving the transformation of magnetic configurations. In contrast, the M_1 mode involves magnetization oscillations distributed over both tori and would require substantially higher field amplitudes to produce switching. The selection of the M_2 mode thus ensures selective, energy-efficient control of the vortex chirality. The procedure involved activating the oscillating magnetic field for 1 nanosecond [45], followed by deactivation, during which the magnetization was observed for 20 ns. To justify the choice of the pulse duration, we additionally explored the effect of varying the excitation time in the range from 0.5 ns to 2.0 ns for representative cases ($\delta = 0.5$), as shown in Fig. S9 in the Supplementary Material. We found that the homochiral-to-heterochiral switching is only achieved for pulse durations around 1 ns within the field amplitudes considered in this work. Shorter pulses do not inject enough energy to overcome the energy barrier separating the two chiral states, while significantly longer pulses may also enable the transition but were not systematically analyzed here. This result indicates that the chirality switching process is highly sensitive to the pulse duration. A more comprehensive study, including a phase diagram of switching as a function of pulse duration and field amplitude, will be the subject of future work. In this stage, we consider the case $\delta = 0.5$, which represents an intermediate magnetic interaction regime between neighboring nanotori, and we set the Gilbert damping constant to $\alpha = 0.01$ [46,47]. To induce the transformation from homochiral nanovortices to heterochiral nanovortices (See Fig. 4(a)), we apply an oscillating field with $f = 14.58$ GHz during 1 ns, and then turn off the field to allow the system to stabilize. By systematically varying the field amplitude B_0 from 100 mT to 1000 mT, we observe that the system switches from the homochiral to the heterochiral configuration when B_0 reaches 700 mT.

Conversely, the reverse transformation-from heterochiral to homochiral nanovortices (See Fig.4(b))-can also be achieved by selecting the appropriate spin-wave frequency and field strength. In this case, we employ an oscillating field at $f = 14.26$ GHz with the same temporal protocol: the field is applied for 1ns and then removed, while the amplitude B_0 is varied. We find that the system transitions back to the homochiral state when B_0 reaches 530 mT. These results demonstrate that the chirality of the nanotorus system can be controlled by tailoring the frequency and amplitude of an external oscillating magnetic field, revealing a tunable mechanism for manipulating topological states in such nanosystems. Similarly, as shown in Figures S4 and S5 of the Supplementary Materials, we demonstrate the transformation between homochiral and heterochiral vortices and vice versa. For $\delta = 0.2$, we report a magnetic field strength of 320 mT for the transition from homochiral to heterochiral vortices and 190 mT for the transition from heterochiral to homochiral vortices. For $\delta = 0.8$, the reported values are 950 mT for the transformation from homochiral to heterochiral vortices and 980 mT for the reverse transition from heterochiral to homochiral vortices.

In addition, we quantified the total energy variation during the transitions between homochiral and heterochiral vortex configurations to estimate the energy barriers governing these processes. The temporal evolution of the total energy under resonant field excitation (see Fig. S6 in the Supplementary Material) shows a well-defined maximum corresponding to the transition barrier $E_{barrier}$. The observed trend reflects the strengthening of magnetostatic coupling between the tori, which requires higher excitation fields to overcome the barrier separating the two chiral states.

4. Conclusion

Our results demonstrate the dynamics of spin waves in concentric nanotori structures using micromagnetic simulations under perpendicular magnetic field pulses. It was observed that the magnetic configuration of the vortices-homochiral or heterochiral-strongly influences the spectrum of resonance modes. In homochiral configurations, the modes tend to converge to a single frequency as the interaction parameter δ increases, whereas in heterochiral configurations, the modes diverge more sharply. Two predominant resonant modes were identified: one located on the outer surfaces of the tori and another concentrated in the inner torus.

A key result of this work is the demonstration that reversible transitions between homochiral and heterochiral states can be induced by applying oscillating magnetic fields tuned in frequency and intensity. For example, for $\delta = 0.5$, homochiral-to-heterochiral switching was achieved by applying a field of 700 mT at 14.58 GHz, and the reverse transition was achieved with 530 mT at 14.26 GHz. This phenomenon was also observed for other δ values, demonstrating the existence of precise field thresholds that allow topological control of the system's magnetic texture.

Furthermore, the estimation of the transition energy barriers revealed that the energetic cost of switching between homochiral and heterochiral configurations increases with the coupling parameter δ, confirming that magnetostatic interactions play a dominant role in stabilizing the vortex chirality.

The quest to control magnetic states has been explored in systems such as magnetic nanodisks and vortex pairs using gigahertz magnetic pulses and laser-assisted switching [48–50], which demonstrates the interest in this topic from a materials engineering perspective. Our results show that magnetic nanostructures shaped like nanotori open up a new line for engineering functional magnetic materials with topological control at the nanometer scale. This advance represents a breakthrough in the integration of 3D geometries into storage technologies, reconfigurable logic, and advanced spintronics.

CRediT authorship contribution statement

Eduardo Saavedra: Writing – original draft, Methodology, Investigation; **Ulises J. Guevara:** Writing – original draft, Investigation; **Carlos Saji:** Validation, Methodology, Investigation; **Tamara González-Vega:** Validation, Investigation; **Pablo Díaz:** Writing – review & editing, Validation, Investigation; **Laura M. Pérez:** Validation, Investigation, Funding acquisition.

Data availability

The data that support the findings of this study are available from the corresponding author upon reasonable request.

Declaration of competing interest

The authors declare that they have no known competing financial interests or personal relationships that could have appeared to influence the work reported in this paper.

Acknowledgements

E.S. and C.S acknowledges the support from Proyecto CORFO/ANID Science UP "Impulsando capacidades de innovación, emprendimiento y transferencia tecnológica para el desarrollo del país", código 20CEIN2-142145. P.D. and L.M.P. acknowledge partial financial support from FONDECYT 1231020. LMP acknowledges partial financial support from Centers of Excellence with BASAL/ANID CIA250002, CEDENNA.

Supplementary material

Supplementary material associated with this article can be found, in the online version, at 10.1016/j.cjph.2025.12.035

References

[1] C. Jin, S. Li, H. Zhang, R. Wang, J. Wang, R. Lian, P. Gong, X. Shi, Spin-wave modes of magnetic bimerons in nanodots, New J. Phys. 24 (7) (2022) 073013.
[2] A.G. Silva-Junior, S.F. de Souza, A.W. Teixeira, D. Laroze, A.R. Pereira, J.M. Fonseca, V.L. Carvalho-Santos, Bimeron stability and non-reciprocal energy behavior in magnetic nanodots, Appl. Phys. Lett. 125 (25) (2024).
[3] N. Arora, Y. Kumar, P. Das, Spin wave behavior and controlled switching of a novel non-trivial magnetic texture in Co/Pt nanodiscs, APL Mater. 13 (4) (2025).
[4] B. Hussain, M. Cottam, Spin waves in ferromagnetic nanorings with interfacial Dzyaloshinskii–Moriya interactions: II. directional effects, Nanomaterials 14 (3) (2024) 286.
[5] J. Gao, R. Zhang, M. Liu, J. Wang, L. Tong, M. Ge, W. Meng, X. Zhou, Z. Liu, Y. Ren, Configurational spin-state evolution during magnetization reversal in coupled Ni80Fe20 multi-nanorings, J. Magn. Magn. Mater. 629 (2025) 173352. https://doi.org/10.1016/j.jmmm.2025.173352
[6] A.V. Sadovnikov, A.A. Zyablovsky, A.V. Dorofeenko, S.A. Nikitov, Exceptional-point phase transition in coupled magnonic waveguides, Phys. Rev. Appl. 18 (2) (2022) 024073.
[7] E.N. Beginin, A.V. Sadovnikov, Y.P. Sharaevsky, S.A. Nikitov, Multimode surface magnetostatic wave propagation in irregular planar YIG waveguide, Solid State Phenomena 215 (2014) 389–393.
[8] A.V. Sadovnikov, K.V. Bublikov, E.N. Beginin, S.A. Nikitov, The electrodynamic characteristics of a finite-width metal/dielectric/ferroelectric/dielectric/metal layer structure, J. Commun. Technol. Electron. 59 (9) (2014) 914–919.
[9] A.V. Sadovnikov, A.A. Grachev, S.A. Odintsov, A.A. Martyshkin, V.A. Gubanov, S.E. Sheshukova, S.A. Nikitov, Neuromorphic calculations using lateral arrays of magnetic microstructures with broken translational symmetry, JETP Lett. 108 (5) (2018) 312–317.
[10] G. Gubbiotti, A. Sadovnikov, E. Beginin, S. Nikitov, D. Wan, A. Gupta, S. Kundu, G. Talmelli, R. Carpenter, I. Asselberghs, et al., Magnonic band structure in vertical meander-shaped Co 40 Fe 40 B 20 thin films, Phys. Rev. Appl. 15 (1) (2021) 014061.
[11] G. Gubbiotti, A. Sadovnikov, E. Beginin, S. Sheshukova, S. Nikitov, G. Talmelli, I. Asselberghs, I.P. Radu, C. Adelmann, F. Ciubotaru, Magnonic band structure in CoFeB/Ta/NiFe meander-shaped magnetic bilayers, Appl. Phys. Lett. 118 (16) (2021).
[12] M.I. Sloika, Y. Gaididei, V.P. Kravchuk, O.V. Pylypovskyi, D. Makarov, D.D. Sheka, Magnetic vortex dynamics on a spherical cap, Low Temp. Phys. 51 (6) (2025) 700–707.
[13] G. Niraula, D. Toneto, G.F. Goya, G. Zoppellaro, J.A.H. Coaquira, D. Muraca, J.C. Denardin, T.P. Almeida, M. Knobel, A.I. Ayesh, et al., Observation of magnetic vortex configuration in non-stoichiometric Fe 3 O 4 nanospheres, Nanoscale Adv. 5 (18) (2023) 5015–5028.
[14] J.D. Alzate-Cardona, D. Sabogal-Suárez, E. Restrepo-Parra, Magnetization switching process in a torus nanoring with easy-plane surface anisotropy, J. Magn. Magn. Mater. 442 (2017) 231–235. https://doi.org/10.1016/j.jmmm.2017.06.130
[15] R.M. Corona, E. Saavedra, S. Castillo-Sepulveda, J. Escrig, D. Altbir, V.L. Carvalho-Santos, Curvature-induced stabilization and field-driven dynamics of magnetic hopfions in toroidal nanorings, Nanotechnology 34 (16) (2023) 165702.
[16] U. Guevara, E. Saavedra, L. Pedraja-Rejas, M.-A. Garrido-Tamayo, S. Aranzubia, E. Cisternas, P. Díaz, D. Laroze, Impact of chirality on the dynamic susceptibility of concentric nanotori, Nanomaterials 15 (13) (2025). https://doi.org/10.3390/nano15130989
[17] G.R. Lewis, J.C. Loudon, R. Tovey, Y.-H. Chen, A.P. Roberts, R.J. Harrison, P.A. Midgley, E. Ringe, Magnetic vortex states in toroidal iron oxide nanoparticles: combining micromagnetics with tomography, Nano Lett. 20 (10) (2020) 7405–7412.
[18] Z. Gao, F. Wang, X. Zhao, T. Wang, J. Hu, P. Yan, Interplay between spin wave and magnetic vortex, Phys. Rev. B 107 (21) (2023) 214418.
[19] S.M. Alam, S. Ikegawa, K. Nagel, F. Mancoff, M. DeHerrera, F. Neumeyer, J.T. Williams, I. Rahman, A. Shah, Y. Kim, et al., Versatile STT-MRAM architecture for memory and emerging applications, in: 2023 IEEE 34th Magnetic Recording Conference (TMRC), IEEE, 2023, pp. 1–2.
[20] M. Endo, M. Al-Mahdawi, M. Oogane, Y. Ando, Control of sensitivity in vortex-type magnetic tunnel junction magnetometer sensors by the pinned layer geometry, J. Phys. D Appl. Phys. 55 (19) (2022) 195001.
[21] S. Zuo, H. Heidari, D. Farina, K. Nazarpour, Miniaturized magnetic sensors for implantable magnetomyography, Adv. Mater. Technol. 5 (6) (2020) 2000185.
[22] S.M. Yakout, Spintronics: future technology for new data storage and communication devices, J. Supercond. Novel Magn. 33 (9) (2020) 2557–2580.
[23] M.A. Khan, J. Sun, B. Li, A. Przybysz, J. Kosel, Magnetic sensors-A review and recent technologies, Eng. Res. Express 3 (2) (2021) 022005.
[24] P. Bhattacharjee, S. Barman, Three-input magnetic logic gates using magnetic vortex transistor, phys. Status Solidi (a) 219 (22) (2022) 2200397.
[25] W. Yu, J. Lan, J. Xiao, Magnetic logic gate based on polarized spin waves, Phys. Rev. Appl. 13 (2) (2020) 024055.
[26] A. Hanif, A.A. Rahim, H. Maab, Vortex dynamics in a spin valve nanopillar having hybrid polarizer and magnetostatic coupling, Phys. B 668 (2023) 415203.
[27] C. Yun, Y. Wu, Z. Liang, W. Yang, H. Du, S. Liu, J. Han, Y. Hou, J. Yang, Z. Luo, Magnetic anisotropy-controlled vortex nano-oscillator for neuromorphic computing, Front. Phys. 10 (2022) 1019881.
[28] C. McKeever, F.Y. Ogrin, M.M. Aziz, Dynamic susceptibility of concentric permalloy rings with opposite chirality vortices, J. Appl. Phys. 121 (20) (2017) 203901.
[29] R. Sahu, A.P. Kotti, P. Tandon, A.C. Mishra, Static and dynamic magnetic characteristics in concentric permalloy nanorings, J. Magn. Magn. Mater. 581 (2023) 170973.
[30] Y. Zhan, L. Deng, W. Dai, Y. Qiu, S. Sun, D. Sun, B. Hu, J. Guan, Fabrication of large-area nanostructures using cross-nanoimprint strategy, Nanomaterials 14 (12) (2024) 998.
[31] J. Askey, A. van den Berg, S.R. Gomez, C. Donnelly, D. Grundler, S. Ladak, Exploiting two-photon lithography, deposition, and processing to realize complex 3D magnetic nanostructures, Adv. Funct. Mater. (2025). https://doi.org/10.1002/adfm.202516383
[32] A. Vansteenkiste, J. Leliaert, M. Dvornik, M. Helsen, F. Garcia-Sanchez, B.V. Waeyenberge, The design and verification of Mumax3, AIP Adv. 4 (107133) (2014). https://doi.org/10.1063/1.4899186
[33] M.-A. Garrido-Tamayo, E. Saavedra, C. Saji, U. Guevara, L.M. Pérez, L. Pedraja-Rejas, P. Díaz, D. Laroze, Stability and spin waves of skyrmion tubes in curved FeGe nanowires, Nanomaterials 14 (18) (2024) 1468.

[34] E. Saavedra, D. Altbir, J. Escrig, S. Castillo-Sepúlveda, R.M. Corona, V.L. Carvalho-Santos, Exploring hopfion stability and dynamics in ring-like structures, Results Phys. 62 (2024) 107835. https://doi.org/10.1016/j.rinp.2024.107835

[35] E. Saavedra, F. Tejo, N. Vidal-Silva, J. Escrig, Symmetry breaking-induced resonance dynamics in bloch point nanospheres: unveiling magnetic volume effects and geometric parameters for advanced applications in magnetic sensing and spintronics, ACS Appl. Mater. Interfaces 16 (21) (2024) 27605–27613. https://doi.org/10.1021/acsami.4c01963

[36] J. Fullerton, A. Hierro-Rodriguez, C. Donnelly, D. Sanz-Hernández, L. Skoric, D.A. MacLaren, A. Fernández-Pacheco, Controlled evolution of three-dimensional magnetic states in strongly coupled cylindrical nanowire pairs, Nanotechnology 34 (12) (2023) 125301.

[37] S. Castillo-Sepúlveda, R.M. Corona, E. Saavedra, D. Laroze, A.P. Espejo, V.L. Carvalho-Santos, D. Altbir, Nucleation and stability of toron chains in non-centrosymmetric magnetic nanowires, Nanomaterials 13 (12) (2023).

[38] S. Lendinez, M.T. Kaffash, O.G. Heinonen, S. Gliga, E. Iacocca, M.B. Jungfleisch, Nonlinear multi-magnon scattering in artificial spin ice, Nat. Commun. 14 (1) (2023) 3419.

[39] M. Kuchibhotla, A. Talapatra, A. Haldar, A.O. Adeyeye, Magnetization dynamics of single and trilayer permalloy nanodots, J. Appl. Phys. 130 (8) (2021).

[40] E. Saavedra, S. Castillo-Sepúlveda, R.M. Corona, D. Altbir, J. Escrig, V.L. Carvalho-Santos, Influence of curvature on the dynamical susceptibility of bent nanotubes, Results Phys. 35 (2022) 105290.

[41] J. Fassbender, J. Von Borany, A. Mücklich, K. Potzger, W. Möller, J. McCord, L. Schultz, R. Mattheis, Structural and magnetic modifications of Cr-implanted permalloy, Phys. Rev. B-Condensed Matter Mater. Phys. 73 (18) (2006) 184410.

[42] K. Wagner, L. Körber, S. Stienen, J. Lindner, M. Farle, A. Kákay, Numerical ferromagnetic resonance experiments in nanosized elements, IEEE Magn. Lett. 12 (2021) 1–5.

[43] C. Wen-Bing, H. Man-Gui, Z. Hao, O. Yu, D. Long-Jiang, Micromagnetic simulation on the dynamic susceptibility spectra of cobalt nanowires arrays: the effect of magnetostatic interaction, Chin. Phys. B 19 (8) (2010) 087502.

[44] E. Saavedra, N. Vidal-Silva, J. Escrig, Dynamic susceptibility of permalloy wire-tube nanostructures, Results Phys. 31 (2021) 104874.

[45] H. Vigo-Cotrina, A.P. Guimarães, Creating skyrmions and skyrmioniums using oscillating perpendicular magnetic fields, J. Magn. Magn. Mater. 507 (2020) 166848. https://doi.org/10.1016/j.jmmm.2020.166848

[46] H. Vigo-Cotrina, S. Urcia-Romero, A. P. Guimarães, Influence of perpendicular uniaxial anisotropy on the switching of a magnetic vortex, J. Appl. Phys. 137 (1) (2025) 013909. https://doi.org/10.1063/5.0243258

[47] H. Vigo-Cotrina, A.P. Guimarães, Switching of skyrmioniums induced by oscillating magnetic field pulses, J. Magn. Magn. Mater. 509 (2020) 166895. https://doi.org/10.1016/j.jmmm.2020.166895

[48] M. Stebliy, A. Jenkins, L. Benetti, E. Paz, R. Ferreira, Non-volatile analog control and reconfiguration of a vortex nano-oscillator frequency, Adv. Funct. Mater. 34 (40) (2024). https://doi.org/10.1002/adfm.202405776

[49] P. Gypens, J. Leliaert, G. Schütz, B. Van Waeyenberge, Commensurate vortex-core switching in magnetic nanodisks at gigahertz frequencies, Phys. Rev. B 105 (9) (2022). https://doi.org/10.1103/physrevb.105.094420

[50] C. Liu, X. Hu, Z. Li, X. Cao, X. Fu, A strategy for fast and precise control of polarity and chirality in magnetic vortices, Front. Phys. 20 (2) (2025). https://doi.org/10.15302/frontphys.2025.022201